JOURNAL OF MATERIALS SCIENCE **33** (1998) 5177–5183

Measurement of stress relaxation in broken fibers embedded in epoxy using Raman spectroscopy

T. MIYAKE
Nagoya Municipal Industrial Research Institute, 3-4-41, Rokuban, Atsuta-ku, Nagoya 456-0058, Japan
E-mail: miyake@nmiri.city.nagoya.jp

T. YAMAKAWA, N. OHNO
Department of Mechanical Engineering, Nagoya University, Furo-cho, Chikusa-ku, Nagoya 464-8603, Japan

Raman spectroscopy was used to study the stress relaxation in broken fibers in a unidirectional composite. A single-fiber model composite consisting of a high modulus PAN-based carbon fiber and an epoxy resin matrix was loaded incrementally until the fiber got broken. Then the stress profile in the broken fiber was monitored under constant overall strain for 1000 hours by determining fiber stress through the stress dependence of the 2700 cm^{-1} Raman band peak position. Three experiments were done at different overall strains. It was observed that the stress profile in each broken fiber changed only a little even after 1000 hours whereas matrix normal stress in the fiber direction relaxed to about a quarter of the initial value in about 200 hours. It is shown that this result does not support linear viscoelastic solutions based on perfect bonding at interface since the present experiments had interfacial debonding and matrix shear yielding around fiber breaks.

1. Introduction

Polymer matrix and metal matrix unidirectional composites reinforced with continuous fibers can be subjected to rupture in longitudinal creep even if the fibers do not creep at all [1–6]. It is obvious that matrix viscosity and stochastic fiber fracture play important roles in such creep rupture. One of the possible mechanisms for the creep rupture is the stress relaxation in broken fibers, as was studied first by Lifshitz and Rotem [1]: As shear creep occurs in the matrix around fiber breaks, the stress in broken fibers relaxes. Then, the neighboring intact fibers are overloaded to induce further fiber breaks, and consequently the composites can be ruptured in longitudinal creep.

The stress relaxation in broken fibers has been studied analytically or numerically in several works so far: Lifshitz and Rotem [1] analyzed the stress relaxation in broken fibers in unidirectional glass fiber reinforced plastics by employing the Laplace transformation for linear viscoelastic problems, and then they evaluated the rupture time in longitudinal creep of such composites by extending the rupture model of Rosen [7]. More detailed analyses for the fiber stress profiles around fiber breaks in unidirectional fiber reinforced plastics were made subsequently within the framework of the shear lag assumption by Lagoudas *et al*. [8] and Mason *et al*. [9]. Phoenix *et al*. [2] and Otani *et al*. [3] performed creep experiments of carbon fiber/epoxy microcomposites, and they analyzed successfully the experimental results using a model which involves a Weibull distribution of fiber strength and micromechanical stress redistribution around fiber breaks. For metal matrix composites, on the other hand, numerical simulations concerning the time-dependent change of stress profiles in broken fibers were done by Goda [10], Kelly and Barbero [11], and Du and McMeeking [12]. Analytical models were then developed and verified on the basis of Du and McMeeking's simulations by Ohno and Yamakawa [13], Iyengar and Curtin [14], and Ohno and Miyake [15].

In spite of the above extensive studies, further works, especially experiments to observe the stress relaxation, seem to be necessary. This is because different tendencies have been predicted on the basis of different assumptions. For example, according to the linear viscoelastic solutions of Lifshitz and Rotem [1] and Lagoudas *et al*. [8], stress redistributes significantly in broken fibers just after fiber breaks. In the numerical analysis of Du and McMeeking [12], on the other hand, stress in broken fibers in a power-law creeping matrix relaxes very slowly in comparison with the matrix normal stress in the fiber direction, as was expressed analytically in a simple form later by Ohno and Miyake [15].

For fibers in a transparent matrix, Raman spectroscopy can be used to measure the stress distributions in them on the basis of the principle that the Raman lines shift with applied stress or strain. This method, which was initiated by Galiotis *et al*. [16], has a feature that a Raman spectrometer equipped with an optical microscope enables us to determine local stress

with high spatial resolution. The method has been employed for measuring the stress distributions in broken fibers in model composite specimens in several works [16–24]. The previous works, however, dealt with the stress distributions just after fiber breaks. It is therefore worthwhile to apply Raman spectroscopy to studying the time-dependent evolution of stress profiles in broken fibers.

The present work is concerned with measurement of the stress relaxation in broken fibers in single-fiber model composite specimens consisting of a high modulus polyacrylonitrile (PAN)-based carbon fiber and an epoxy resin matrix. The work is featured by long term monitoring of the stress profiles in broken fibers using Raman spectroscopy. The profiles of interfacial shear stress are also determined from those of fiber stress. On the basis of the experimental observations, then, the effect of interfacial debonding and matrix shear yielding on the stress relaxation in broken fibers is discussed in comparison with linear viscoelastic analysis based on perfect bonding at interface.

2. Experimental procedure

2.1. Materials used and specimen preparation

The fibers employed in the study were commercially available high modulus PAN-based carbon fibers (SR-40K, Mitubishi Rayon Co. Ltd.). The fibers had been subjected to a surface treatment of epoxy compatible oxidation sizing. The matrix was a room-temperature curing bisphenol A-based epoxy resin AER260 mixed with a polyamine hardener HY847 in the 10 : 4 weight proportion. Both AER260 and HY847 were obtained from Asahi-Ciba Ltd. Some mechanical properties of the fibers and the matrix are given in Table I. It is noticed that the fiber properties in the table, which were measured using polymer impregnated strands, apply only approximately to monolithic fibers. The fiber diameter was determined to be 5.2 μm from a scanning electron microscope photograph of a fiber embedded in the epoxy resin.

The single-fiber composite specimens used in the study were prepared as follows: The epoxy resin, which was mixed thoroughly with the hardener and then degassed in a vacuum, was cast into rectangular molds until the molds got half full with it. The epoxy resin in the molds was then subjected to curing at room temperature for 24 h. Subsequently, a fiber was put on the epoxy resin in each mold, and the molds were topped up with the epoxy resin. Then, after curing at room temperature for 7 days, the single-fiber composite samples in the molds were machined into dog-bone shaped

TABLE I Mechanical properties of carbon fiber and epoxy resin

	Carbon fiber (SR-40K)	Epoxy resin (AER260/HY847)
Young's modulus (GPa)	490*	3.7
Tensile strength (GPa)	4.3*	0.057
Elongation (%)	0.9*	2.0

*Measured using polymer impregnated strands.

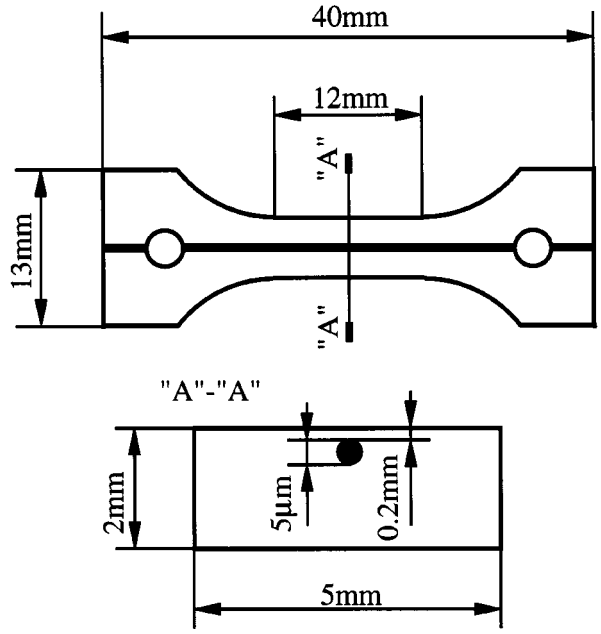

Figure 1 Shape of single-fiber composite specimens for stress relaxation tests.

specimens with the fibers aligned to the axial direction at a depth of 200 μm from the top surfaces (Fig. 1). The specimens were polished with 0.01 μm alumina slurry, so that they became smooth and transparent enough to prevent attenuation of the scattered light from fibers.

2.2. Raman spectroscopy measurement

Raman spectra were measured using a micro-Raman spectrometer (Model 750-1, Instruments S. A. Inc.) equipped with a single polychromater coupled to a modified optical microscope. Fig. 2 shows the block diagram of the Raman spectrometer. An Ar^+ laser operating at 514.5 nm was employed as the light source. The laser beam was focused to an about 1 μm spot on the fiber surface using a microscope objective of $\times 80$. The power of the incident light to the fiber surface was retained below 1 mW for the purpose of avoiding peak shifting of Raman spectra as well as fiber damage due to local overheating. The backscattered light was dispersed by leading it to the spectrometer through the microscope objective. Raman spectra were recorded using a charge coupled device (CCD) cooled with liquid

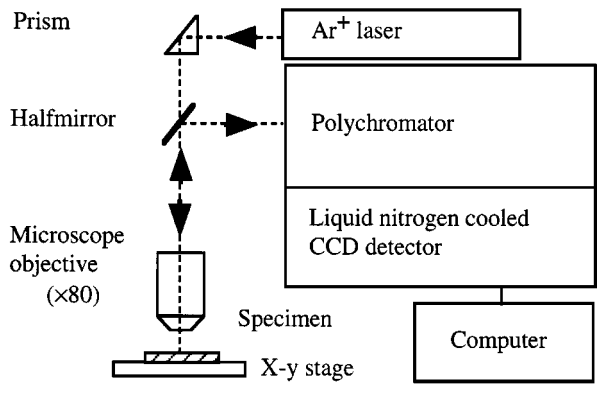

Figure 2 Micro-Raman spectroscopic system.

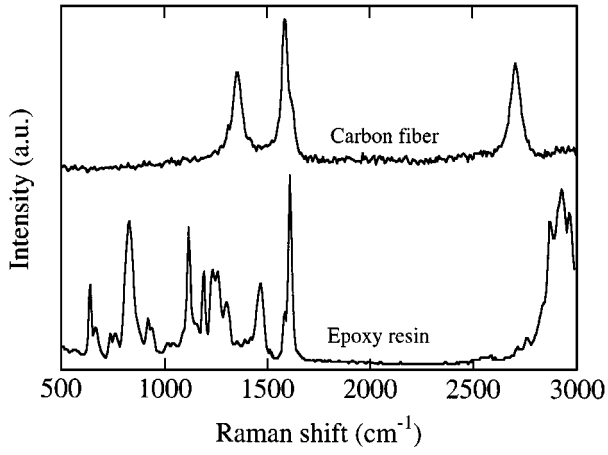

Figure 3 Raman spectra of free-standing carbon fiber and epoxy resin.

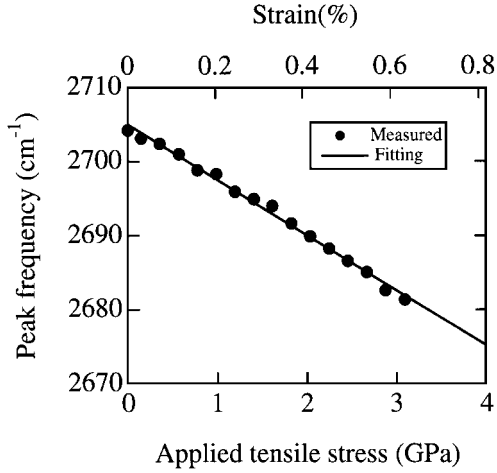

Figure 5 Dependence of 2700 cm^{-1} Raman band peak position on applied tensile stress.

nitrogen. The peak frequencies of Raman spectra were determined by fitting the raw data with the Lorentzian distribution function, and then they were rectified using a neon light source as a reference to remove the fluctuation with time. Thus the peak positions, i.e., Raman frequencies, of the Raman bands were obtained with an accuracy better than ± 0.5 cm^{-1}.

The Raman spectra obtained respectively from a free-standing carbon fiber and from the epoxy resin are shown in Fig. 3. The fiber exhibited two major peaks at 1580 and 2700 cm^{-1} whereas the epoxy resin had many peaks in the zone smaller than 1600 cm^{-1}. For the fibers in the model composite specimens, therefore, the second-order peak around 2700 cm^{-1} was regarded as appropriate for monitoring the stress-induced peak frequency shifting, because the first-order peak around 1580 cm^{-1} was superimposed almost completely by a peak of the scattered light from the epoxy resin. Fig. 4 shows the Raman spectrum near 2700 cm^{-1} obtained from the carbon fiber in one of the composite specimens. It is seen from the figure that although the spectrum was affected by the epoxy resin, the Lorenzian curve fitting allowed us to determine accurately the peak position in the 2700 cm^{-1} band of the carbon fiber by removing the two, weak spectra of the epoxy resin.

The stress dependence of the peak position in the 2700 cm^{-1} Raman band for the carbon fibers employed was determined by taking Raman spectra of a single fiber stressed incrementally with dead weights in air. The peak position ν was found to shift almost linearly with applied tensile stress σ_f, as shown in Fig. 5. Using the least squares method, the relation between ν and σ_f was fitted as

$$\nu = 2705.0 \pm 0.2 - (7.5 \pm 0.1)\sigma_f, \qquad (1)$$

where ν and σ_f are given in cm^{-1} and GPa, respectively.

The above relation was ascertained to be applicable to the fibers in the composite specimens: By loading incrementally one of the specimens, the peak position ν in the 2700 cm^{-1} Raman band of the embedded fiber was measured until the fiber got broken. Then, ν was converted to fiber strain using Equation 1 and Hooke's law. The resulting fiber strain was compared with the axial strain measured with strain gauges adhered to the specimen top surface, which was very close to the fiber (Fig. 1). As shown in Fig. 6, the strains agreed well with each other. Equation 1 was thus found valid to the fibers in the composite specimens as well.

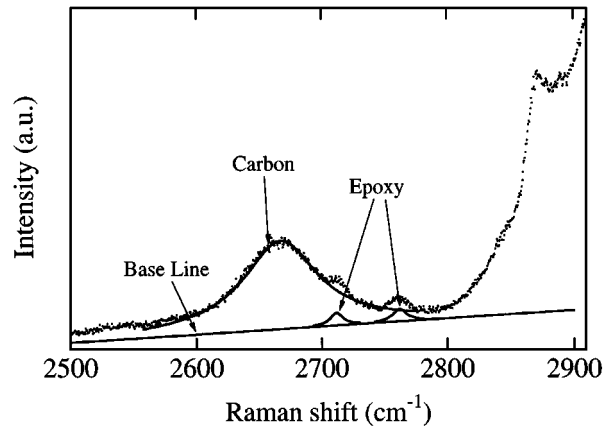

Figure 4 Raman spectrum for 2700 cm^{-1} Raman band of carbon fiber embedded in epoxy resin subjected to 1.0% axial strain, together with fitted Lorentzian curves.

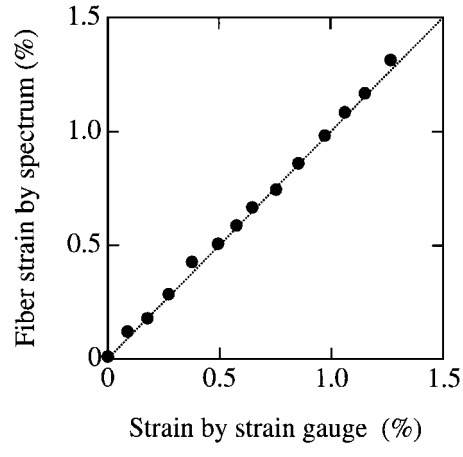

Figure 6 Comparison between fiber and overall strains in a composite specimen measured using Raman spectroscopy and strain gauges, respectively.

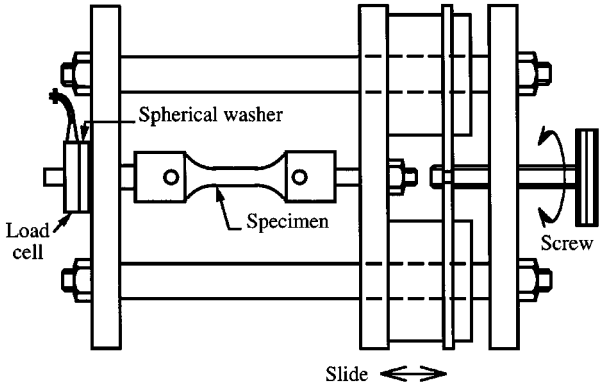

Figure 7 Loading device for stress relaxation tests.

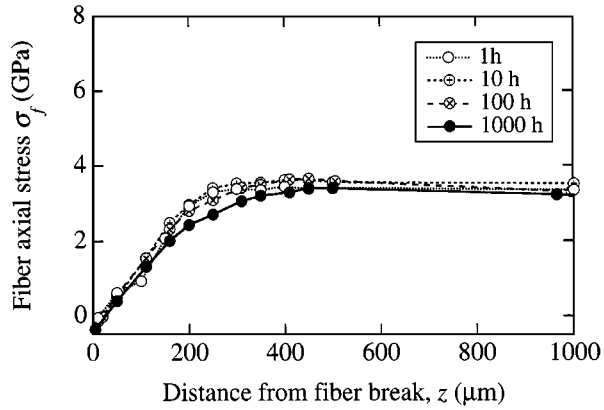

Figure 8 Distribution of axial stress in broken fiber at $\varepsilon = 0.7\%$.

2.3. Stress relaxation tests

Each specimen was elongated in the fiber direction by means of a straining rig shown in Fig. 7. The rig was mounted directly on the microscope stage in the Raman system. The axial strain, measured with strain gauges adhered to the top surface of the specimen, was increased stepwise by 0.1% increments. After every increment the fiber was inspected within about ±2.5 mm distances from the specimen center by inserting a polarizer into the microscope of the Raman system. As soon as the fiber was found fractured, the axial strain was kept constant for 1000 h in air, which was conditioned to be 25 °C and dehumidified to have the relative humidity below 50%. While holding the axial strain, the fiber was scanned in the axial direction at appropriate times using the Raman microprobe; i.e., the Raman frequency in the 2700 cm^{-1} band was measured at points spaced at intervals of 50 μm within a 1000 μm distance from a break of the fiber. Using Equation 1, then, the frequency was converted to fiber stress σ_f to obtain the stress distribution in the fiber near the break. It is noticed that before scanning the fiber, the Raman frequency was measured tentatively at a few points about 1000 μm apart from the break, and the axial strain to be kept constant was modified slightly, so that at such remote points the fiber strain determined from the Raman frequency fluctuated negligibly with time.

The axial force induced in the specimen was monitored continuously by a load cell connected in series to the specimen in the straining rig (Fig. 7). The force was divided by the cross-sectional area in the gauge section to evaluate the matrix tensile stress in the fiber direction. This matrix stress, which was an averaged one in the gauge section, is simply referred to as matrix normal stress and indicated as σ_m from now on.

3. Results

Three specimens were subjected to constant overall strain for 1000 h, as was described in the previous section. The fibers in them got fractured when the axial strain measured with strain gauges, ε, was increased respectively to 0.7, 1.0 and 1.4%. The experiments of $\varepsilon = 0.7$ and 1.0% had similar results. Hence only the experiments of $\varepsilon = 0.7$ and 1.4%, which had very different results, are reported here to save the space.

3.1. Stress relaxation at 0.7% constant strain

Fig. 8 shows the axial stress profiles in the broken fiber at the elapsed times of $t = 1$, 10, 100 and 1000 h after the fiber break in the experiment of $\varepsilon = 0.7\%$. The following features are seen from the figure: Fiber stress σ_f, which was zero at the break, recovered the stress in intact fibers, about 3.4 GPa, with the increase of the distance z from the break. The stress profiles at $t = 1$, 10 and 100 h were almost the same, but from $t = 100$ h to 1000 h stress relaxation occurred a little in the fiber and made stress recovery length increase from about 300 to 400 μm.

The profiles of interfacial shear stress τ around the fiber break were computed from those of σ_f shown in Fig. 8 using an equilibrium equation

$$\tau = \frac{r_f}{2}\frac{\partial \sigma_f}{\partial z}, \tag{2}$$

where r_f denotes the radius of fibers. The differential $\partial\sigma_f/\partial z$ was however found to be affected easily by the errors in measuring σ_f. Savitzky-Golay's coefficient [25] for a quadratic polynomial was therefore employed for smoothing the differential, though it became impossible to evaluate τ at the two points closest to the break. The profiles of τ obtained with such smoothing are shown in Fig. 9. As seen from the figure, τ varied little by little with time, and consequently the maximum

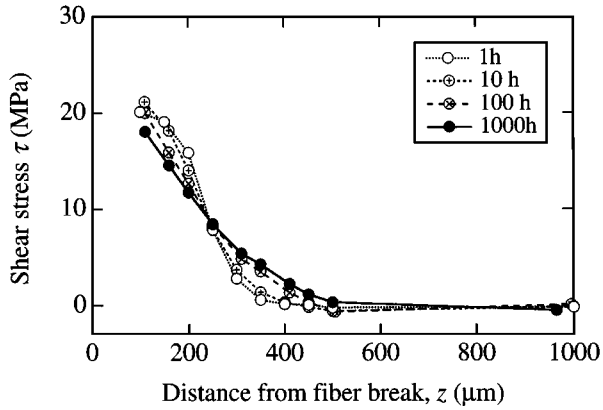

Figure 9 Distribution of interfacial shear stress on broken fiber at $\varepsilon = 0.7\%$.

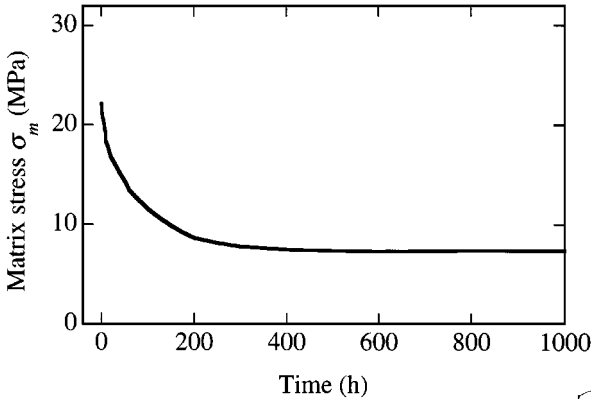

Figure 10 Relaxation of normal stress in matrix, σ_m, at $\varepsilon = 0.7\%$.

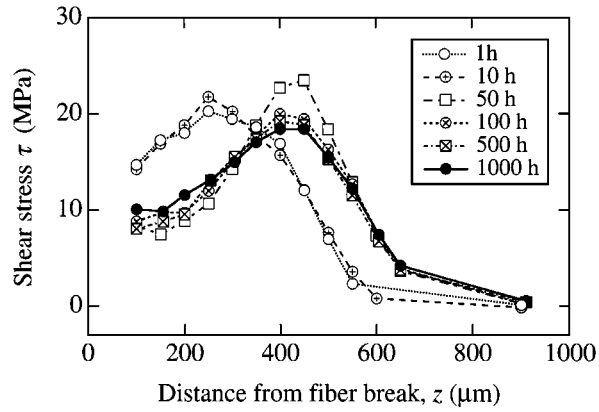

Figure 12 Distribution of interfacial shear stress on broken fiber at $\varepsilon = 1.4\%$.

value of τ decreased by about 10% in 1000 h after the fiber break.

Matrix normal stress σ_m, on the other hand, relaxed very significantly, as shown in Fig. 10. It took only 200 h for σ_m to relax to about one third of the initial value. This relaxation of σ_m was in marked contrast to that of σ_f in the broken fiber.

Therefore we can say that in the experiment of $\varepsilon = 0.7\%$ the relaxation of σ_f in the broken fiber was little and very slow in comparison with that of σ_m. In other words, matrix shear stress around the fiber break relaxed much less significantly than matrix normal stress.

3.2. Stress relaxation at 1.4% constant strain

In another experiment reported here the increase of ε from 1.3 to 1.4% induced three fiber breaks in the observable section within about ±2.5 mm from the specimen center though no fiber break was found there at $\varepsilon = 1.3\%$. The profiles of fiber stress near one of the breaks at $t = 1$, 10, 50, 100 and 1000 h are shown in Fig. 11. As seen from the figure, the experiment had a spontaneous increase of stress recovery length in the time period from $t = 10$ to 50 h. Such an increase, which was not observed in the experiment of $\varepsilon = 0.7\%$, did not take place further after $t = 50$ h till the experiment was terminated at $t = 1000$ h.

The corresponding profiles of interfacial shear stress τ, calculated using Equation 2 from the data of fiber stress, are shown in Fig. 12. The profiles in the figure are characterized by peaks, which were not seen in the experiment of $\varepsilon = 0.7\%$. In each profile τ increased from a relatively low value to a peak then decreased to zero with the increase of z from the break. The peak, which was located at $z \approx 250$ μm at $t = 1$ and 10 h, shifted to $z \approx 450$ μm in the time period from $t = 10$ to 50 h in accordance with the spontaneous increase of stress recovery length seen in Fig. 11. The peak values of τ at $t = 1$ to 50 h were almost the same and a little larger than 20 MPa (Fig. 12). It is appropriate to regard such a value of τ as the shear strength of the carbon/epoxy interface in the present composite, since the break-to-peak sections were found suffering from interfacial debonding by inserting a polarizer into the microscope of the Raman system. We can thus conclude that the increase of stress recovery length mentioned above was due to the propagation of interfacial debonding in the axial direction of the fiber. It is emphasized that the propagation mentioned above took place spontaneously under constant overall strain.

Let us compare the relaxation behaviors of fiber stress σ_f and matrix normal stress σ_m. As seen from Fig. 12, the peak value of τ decreased little by little with time after $t = 50$ h. This means that σ_f had a very weak decrease with time with respect to the maximum gradient in the stress recovery section. On the other hand, σ_m relaxed to about a quarter of the initial value in only 200 h after the fiber break (Fig. 13). Thus the experiment of $\varepsilon = 1.4\%$,

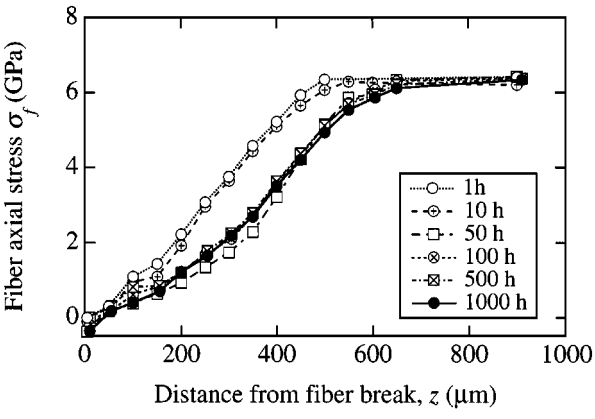

Figure 11 Distribution of axial stress in broken fiber at $\varepsilon = 1.4\%$.

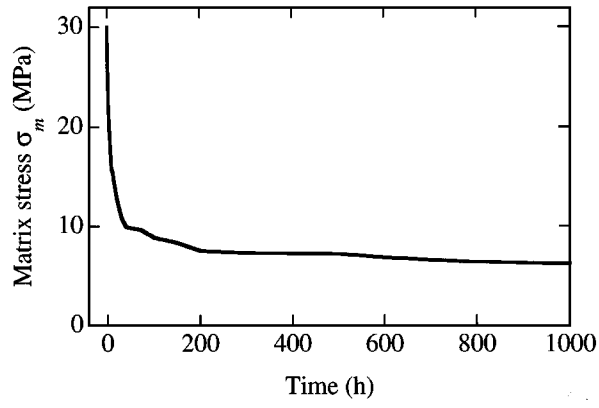

Figure 13 Relaxation of normal stress in matrix, σ_m, at $\varepsilon = 1.4\%$.

in which the propagation of interfacial debonding occurred, also had the feature that σ_m relaxed much more quickly than σ_f in the broken fiber and τ near the break.

4. Discussion

In the present experiments, the fiber stress and interfacial shear stress around fiber breaks relaxed a little and very slowly in comparison with matrix normal stress. This result is now compared qualitatively with linear viscoelastic solutions.

Lifshitz and Rotem [1] pointed out that stress in broken fibers can relax as a result of matrix shear creep around fiber breaks in unidirectional composites subjected to constant overall strain. They considered a long elastic fiber broken in a linear viscoelastic matrix in a cylindrical cell. They obtained approximately an inverse Laplace transformation of the corresponding elastic solution based on a shear lag model, in which perfect bonding at the fiber/matrix interface was assumed prevailing even near the fiber break. They thus showed that the time-dependent extension of stress recovery length, $\delta(t)$, under constant overall strain satisfies

$$\delta(t) \propto \sqrt{J(t)} \tag{3}$$

where $J(t)$ denotes the shear creep compliance of the matrix. This result was almost acertained in detailed numerical analysis [8]. The above equation suggests the following: The time-dependent extension of stress recovery length, i.e., the stress relaxation in broken fibers, takes place as significantly as the relaxation of matrix normal stress σ_m, since the greater the creep compliance $J(t)$ is the more significant the relaxation of σ_m is.

The prediction mentioned above, however, does not agree with the tendency in the present experiments, in which fiber stress relaxed a little and very slowly in comparison with σ_m. This inconsistency is attributable to the assumptions in the analysis, i.e., perfect bonding at the fiber/matrix interface and linear viscoelasticity of the matrix. According to the assumptions, the profile of interfacial shear stress τ just after a fiber break in the cylindrical cell is expressed in the following form, in which the elastic solution of Rosen is modified by taking into account the radial gradient of matrix shear stress in the cell [26]:

$$\tau = E_f \varepsilon \left[\frac{G_m}{2E_f \ln(r_e/r_f)} \right]^{1/2} \exp(-\eta z), \tag{4}$$

where E_f and G_m denote the elastic moduli of fiber tension and matrix shear, respectively, r_e/r_f indicates the ratio of fiber radius to cell radius, and

$$\eta^2 = \frac{2G_m}{r_f^2 \ln(r_e/r_f)}. \tag{5}$$

It is appropriate to take $r_e/r_f \approx 5$ for single-fiber composites such as in the present work [27]. Then, Equation 4 with the material constants in Table I gives the maximum value of τ in the experiment of $\varepsilon = 0.7\%$ as

$$\tau_{max} \approx 100\,\text{MPa}. \tag{6}$$

We notice that the value above is about five times larger than the experimental one obtained just after the break (Fig. 9). This big difference is attributable to matrix shear yielding and interfacial debonding. In addition we notice that matrix shear creep may have some nonlinearity in stress dependence. Then, we are allowed to say as follows: In the present experiments, matrix shear creep around fiber breaks did not occur so significantly as in the analysis of Lifshitz and Rotem, and consequently fiber stress near fiber breaks relaxed very slowly in comparison with matrix normal stress.

5. Conclusions

In this study the stress relaxation in broken fibers in single carbon fiber/epoxy composite specimens subjected to constant overall strain was investigated experimentally using a Raman microprobe. Each specimen was loaded incrementally until the fiber got broken, and subsequently the stress distribution in the broken fiber was monitored under constant overall strain for 1000 hours by determining fiber stress through the stress dependence of the 2700 cm^{-1} Raman band peak position. The results obtained are summarized as follows:

1. In the experiment of 0.7% overall strain, the stress profile in the broken fiber changed only a little even after 1000 hours. Nearly the same relaxation behavior was observed at 1.0% overall strain though not reported in the present paper. In the experiment of 1.4% overall strain, on the other hand, spontaneous increase of stress recovery length occurred as a result of the propagation of interfacial debonding; after the increase, however, the broken fiber had only a little change of stress distribution.
2. Matrix normal stress relaxed to about one third or quarter of the initial value in about 200 hours in the experiments. This relaxation was very significant in comparison with that in broken fibers mentioned above.
3. The maximum value of interfacial shear stress around fiber breaks was much lower than an elastic prediction based on perfect bonding at interface. Such low interfacial shear stress, which is attributable to matrix shear yielding and interfacial debonding around fiber breaks, was regarded as responsible for the little relaxation of stress in broken fibers observed in the experiments.

Acknowledgements

The financial support of the Tatematsu Foundation and the technical support of Mr. Y. Masanaka of Nagoya University are gratefully acknowledged.

References

1. J. M. LIFSHITZ and A. ROTEM, *Fiber Sci. Technol.* **3** (1970) 1.
2. S.L. PHOENIX, P. SCHWARTZ and H. H. ROBINSON IV, *Compos. Sci. Technol.* **32** (1988) 81.

3. H. OTANI, S. L. PHOENIX and P. PETRINA, *J. Mater. Sci.* **26** (1991) 1955.
4. N. OHNO, K. TOYODA, N. OKAMOTO, T. MIYAKE and S. NISHIDE, *J. Eng. Mater. Technol.* **116** (1994) 208.
5. N. OHNO, T. FUJITA and T. MIYAKE, *Mater. Sci. Res. Int.* **2** (1996) 199.
6. C. H. WEBER, Z.-Z. DU and F. W. ZOK, *Acta Mater.* **44** (1996) 683.
7. B. W. ROSEN, *AIAA J.* **2** (1964) 1985.
8. D. C. LAGOUDAS, C.-Y. HUI and S. L. PHOENIX, *Int. J. Solids Struct.* **25** (1989) 45.
9. D. D. MASON, C.-Y. HUI and S. L. PHOENIX, *ibid.* **29** (1992) 2829.
10. K. GODA, in Proceedings of 12th Symposium on Material and Structual Reliability (in Japanese), Kagawa, December 1993 (The Society of Materials Science, Japan, 1993) p. 45.
11. K. W. KELLY and E. BARBERO, *Int. J. Solids Struct.* **30** (1993) 3417.
12. Z.-Z. DU and R. M. MCMEEKING, *J. Mech. Phys. Solids* **43** (1995) 701.
13. N. OHNO and T. YAMAKAWA, *JSME Int. J.* **39**–**A** (1996) 517.
14. N. IYENGAR and W. A. CURTIN, *Acta Mater.* **45** (1997) 3419.
15. N. OHNO and T. MIYAKE, *Int. J. Plast.*, in press.
16. C. GALIOTIS, R. J. YOUNG, P.H.J. YEUNG and D. N. BAECHELDER, *J. Mater. Sci.* **19** (1984) 3640.
17. C. GALIOTIS, *Compos. Sci. Technol.* **42** (1991) 125.
18. C. F. FAN, D. A. WALDMAN and S. L. HSU, *J. Polym. Sci. B, Polym. Phys.* **29** (1991) 235.
19. N. MELANITIS, C. GALIOTIS, P. L. TETLOW and C. K. L. DAVIES, *J. Mater. Sci.* **28** (1993) 1648.
20. Y. H. HUANG and R. J. YOUNG, *Compos. Sci. Technol.* **52** (1994) 505.
21. M. C. ANDREWS and R. J. YOUNG, *J. Mater. Sci.* **30** (1995) 5607.
22. D. T. GRUBB, Z.-F. LI and S. L. PHOENIX, *Compos. Sci. Technol.* **54** (1995) 237.
23. H. D. WAGNER, M. S. AMER and L. S. SCHADLER, *J. Mater. Sci.* **31** (1996) 1165.
24. V. CHOHAN and C. GALIOTIS, *Compos. Sci. Technol.* **57** (1997) 1089.
25. A. SAVITZKY and M. J. E. GOLAY, *Anal. Chem.* **36** (1964) 1627.
26. T. W. CLYNE and P. J. WITHERS, in "An Introduction to Metal Matrix Composites" (Cambridge University Press, London, 1993) p. 23.
27. Z.-F. LI and D. T. GRUBB, *J. Mater. Sci.* **29** (1994) 189.

Received 6 January
and accepted 18 September 1998